Med Biol Eng Comput (2008) 46:233–240
DOI 10.1007/s11517-007-0297-4

ORIGINAL ARTICLE

Fully automated computer algorithm for calculating articular contact points with application to knee biomechanics

Alon Wolf · Branislav Jaramaz · Patricia E. Murtha

Received: 16 February 2007 / Accepted: 24 November 2007 / Published online: 9 January 2008

Abstract A fully automated computer algorithm for calculating the articular contact points between two bone surface models is presented. The algorithm requires the bone surface models and their relative positions as inputs in order to resolve the articular contact path. In the case of surface model overlap due to measurement errors or as a solution of an optimization procedure, the result is a volumetric estimation of the space confined between the two surfaces. The algorithm is based on attaching a grid of lines to one bone surface model and calculating the intersecting points of each of the lines in the grid with both bone surface models. The contact points are then determined as the closest points between the surfaces along the lines in the grid. The same contact points are used to evaluate any volume that is confined between two overlapping surface models. The algorithm is ideal for use in biomechanical studies, simulations of joint motion, and optimizations that require an iterative process to determine contact path and relative bone position. The algorithm is applied to a Sawbones® knee model that is moved from flexion to extension while being tracked by an optical tracking system. The contact path of the two bones is generated and an example of calculating bone impingement is provided.

A. Wolf (✉)
Faculty of Mechanical Engineering,
Technion Israel Institute of Technology,
Haifa 32000, Israel
e-mail: alonw@tx.technion.ac.il

B. Jaramaz · P. E. Murtha
Institute for Computer Assisted Orthopedic Surgery (ICAOS),
The Western Pennsylvania Hospital, Mellon Pavilion, Suite 242,
4815 Liberty Avenue, Pittsburgh, PA 15217, USA

Keywords Knee · Kinematics · Contact points · Contact volume · Contact area · Surface model

1 Introduction

The biomechanical study of joints often requires the calculating of contact points and contact paths of two bone surfaces while being subjected to flexion. Classical examples are knee kinematics studies. The main goal in most knee kinematic research efforts is to create an accurate knee-specific model incorporating geometry and soft and hard tissues properties that can predict knee motion. These mathematical and kinematical models are based on mechanical equilibrium of constraints on the knee [4, 9, 25]. The articular contact points are vital to the solution for these parametric models. This challenge has been addressed by several researchers that estimated the articular contact points by using geometry data of both bones [1–3, 7, 12, 15, 17, 18, 21].

Banks and Hodge [2] and Banks et al. [3] introduced a method that resolved the relative position of two knee implant components with respect to each other from X-ray fluoroscopy images. For their system, the researchers displayed a 3D CAD model of an implant (from a library of templates) as an overlay on the original X-ray images. Then an image-matching algorithm determined the position of the implant. Kinematic parameters such as contact points were measured. Hoff et al. [12] introduced the same concept; however they changed the matching algorithm and the way the template library was presented. Once matching was completed, contact points of the two components were determined along with the area of the contact region and liftoff angle. Komistek et al. [17] and Incavo et al. [15] implemented similar methods of matching 3D models of 2D images and extracting contact points.

DeFrate et al. [7] quantified the contact between the tibia and the femoral cartilage during in vivo knee flexion by using two orthogonal fluoroscopic images and 3D MRI-based computer models of the knee. Once the subject's knee was imaged, the fluoroscopic images were imported to a computer where they were displayed in orthogonal planes. Next, the contact points on the medial and lateral tibial plateau were calculated by finding the centroid of the intersection of the tibial and femoral cartilage layers and by using the bony geometry alone. Scarvell et al. [21] used a 1.5 T closed field MRI unit and a fast gradient echo sequence in order to get the tibiofemoral contact mapping. From the set of knee images for each subject at each position (0°–90° at 15° intervals) an image was chosen which was closest to the center of the medial and lateral components. This chosen image was used to manually record the tibiofemoral contact position. Von Eisenhart-Rothe et al. [23] segmented cartilage structure from MR images in order to determine the tibiofemoral contact point. In slices where contact between the femur and tibia were detected, the two structures were separated by a line of 1 pixel width, thus distinguishing between the two surfaces. To calculate the contact area, the outline of the cartilage that was segmented was expanded by one pixel. All voxels that were segmented in both the femur and the tibia cartilage were then counted. These voxels represented the contact area. Chen et al. [5] calculated the contact location between the femoral and tibial articular surfaces that minimized the strain energy stored in the ligaments of the knee. Their model assumed that the mechanical properties of the ligaments are given.

These studies provide surface model contact points by directly measuring the points on a computer image of the surfaces. Some of the presented algorithms also require preprocessing and segmentation of the relevant data in the images. The fact that these processes were not fully automated, i.e., required user interface and input, makes them inadequate for integration in biomechanical studies that require online, iterative computations that result in the contact points. In this study, we report on a novel, fully automatic computer algorithm that calculates the contact points on both condyles between the tibia and the femur as a function of the bone location. This method requires as input the corresponding surface models of both the tibia and femur (e.g., list of vertices and triangles), and a set of transformation matrices between the two surface models for every flexion angle of interest. For each flexion angle, the algorithm calculates either the point of contact or an estimated volume of intersection between two bones. Without loss of generality, the algorithm is applied to a Sawbones® knee model that is moved from flexion to extension while being tracked by an optical tracking system. The contact path of the two bones is generated and an example of calculating bone impingement is provided.

2 Method

The contact points between the tibia and femur under flexion are vital information for biomechanical studies and simulations of knee motion, as well as for implant design [5]. However, definition of the contact points is not always obvious since the information usually provided is of the surface model of the bones and their relative position (location and orientation). Following is a new approach that calculates contact points between two surface models of bones given their relative configurations. Although we demonstrate our method on the knee, it can be applied to any two moving objects.

2.1 Calculating contact points

For this algorithm, we begin with surface models of both the femur, $\mathcal{M}_{\mathrm{F}}$, and the tibia, $\mathcal{M}_{\mathrm{T}}$, which are given as triangulated meshes of n_{F} and n_{T} triangles respectively, such that:

$$\mathcal{M}_{\mathrm{F}}(\mathcal{V}_{\mathrm{F}}, \mathcal{T}_{\mathrm{F}}) = \bigcup_{i=1}^{n_{\mathrm{F}}} \mathcal{T}_{\mathrm{F},i} \tag{1}$$

and

$$\mathcal{M}_{\mathrm{T}}(\mathcal{V}_{\mathrm{T}}, \mathcal{T}_{\mathrm{T}}) \bigcup_{i=1}^{n_{\mathrm{T}}} \mathcal{T}_{\mathrm{T},i}, \tag{2}$$

where $\mathcal{V}_{\mathrm{F}}$ and $\mathcal{V}_{\mathrm{T}}$ are the respective femur vertices and tibia vertices, and $\mathcal{T}_{\mathrm{F}}$ and $\mathcal{T}_{\mathrm{T}}$ are the respective femur surface triangles and tibia surface triangles. In a general simulation we set one bone as the reference system and describe the motion of the other bone relative to the first. Since for the knee system it is easier to visualize the tibia as moving relative to the femur, we set the femur as the reference system. Next we fix a sampling grid, $\mathcal{P}_{\mathrm{G}}$, of m points to the tibia and attach a set of m parallel lines, $\mathcal{L}$, to the grid such that when the tibia moves through different flexion configurations both the sampling grid and the set of lines attached to it transform with it (Fig. 1a–c). Line direction is defined based on the anatomic reference frame of the tibia(see Fig. 1d, e for the reference frames given in red, green and blue). For every line within the set of lines we then solve for its intersection with the tibia and femur surface models. The points of intersection on the tibia and on the femur formulate two sets of points $\mathcal{P}_{\mathrm{T}}$ and $\mathcal{P}_{\mathrm{F}}$ respectively. We compute the distance along the line between the intersecting points on the tibia and on the femur as:

$$d_j = \left\| \mathcal{P}_{\mathrm{T},j} - \mathcal{P}_{\mathrm{F},j} \right\|_{j=1,\ldots,m} \tag{3}$$

The contact points $\mathcal{P}_{\mathrm{C.T}}$, and $\mathcal{P}_{\mathrm{C.F}}$ are then chosen to be the ones corresponding to the smallest distance d_j. This process is repeated for every flexion configuration.

The flexion configuration is defined by the w homogeneous transformation matrices, ${}^{\mathrm{F}}T_{\mathrm{T},i}$, representing the position and orientation of the tibia in the femur coordinate system for each of the w observations, where ${}^{\mathrm{F}}T_{\mathrm{T},i}$ is given as:

$$ {}^{\mathrm{F}}T_{\mathrm{T},i} = \begin{bmatrix} R_{3\times3} & t_{3\times1} \\ 0_{1,3} & 1 \end{bmatrix} \quad i = 1,\ldots,w. \tag{4} $$

R is the rotation matrix and t is the translation vector between the two coordinate systems.

Since the proposed algorithm is based on manipulating a set of lines and calculating intersection points of each of the lines with a piecewise linear surface, we used *Plücker* line coordinates [16] and line geometry tools [19]. Following is a proposed algorithm as performed on one of the knee condyles:

(a) Define surface models $\mathcal{M}_{\mathrm{F}}$ and $\mathcal{M}_{\mathrm{T}}$ for the femur and tibia, respectively.

(b) Define a sampling grid $\mathcal{P}_{\mathrm{G}}$ of m points and attach it to the tibia such that it is well below the tibia plateau and normal to the z-axis of the tibia coordinate system (Fig. 1d, e). Determine grid spacing as a function of the typical surface model unit size (in our case a triangle) and required output resolution.

(c) Define a set of lines $\mathcal{L}$ such that each line contains one point in $\mathcal{P}_{\mathrm{G}}$ and is parallel to the z-axis of the tibia coordinate system. The lines are represented by their *Plücker* line coordinates [6, 16] such that the j-th line in the set is given by:

$$ \mathcal{L}_j = \left(\hat{Z}_T, \mathcal{P}_{G,j} \times \hat{Z}_T\right) = (l, \bar{l})_i, \quad j = 1,\ldots,m, \tag{5} $$

where $\hat{Z}_{\mathrm{T}}$ is a normal vector parallel to the z-axis in the tibia coordinate system. Note that $\mathcal{L}$ is an $m \times 6$ matrix such that every row in $\mathcal{L}$ is a sextuple vector where the first three components, denoted by l, are the line's direction vector and the other three components, $\bar{l}$, represent the torque that the line exerts with respect to the tibia coordinate system.

(d) Calculate the intersection point of each of the lines in $\mathcal{L}$ with both surface models $\mathcal{M}_{\mathrm{F}}$ and $\mathcal{M}_{\mathrm{T}}$ (Fig. 1d, e). For example, denote the intersecting point of line $\mathcal{L}_j$, with tibia surface model as $S_{\mathrm{T},j}$. $S_{\mathrm{T},j}$ can be calculated as the intersection of $\mathcal{L}_j$ with the plane $U_{\mathrm{T},i}$ which is defined by the triangle $\mathcal{T}_{\mathrm{T},i}$ in$\mathcal{M}_{\mathrm{T}}$ [20]:

$$ \begin{aligned} S_{\mathrm{T},j} &= (s_0, s)_{\mathrm{T,j}} = \left(u_i \cdot l_j, -u_{0,i} l_j + u_i \times \bar{l}_j\right) \\ j &= 1,\ldots,m \quad i = 1,\ldots,n_{\mathrm{F}}, or\ n_{\mathrm{T}}, \end{aligned} \tag{6} $$

where $S_{\mathrm{T},j}\Re = (s_0, s)\Re$ are the homogeneous Cartesian coordinates of a point, and $\Re U_{\mathrm{T},i} = \Re(u_0, u)_{\mathrm{T},i}$ is the homogeneous plane coordinate vector of a plane in the linear space $\Re$. Referring to Fig. 2, since $U_{\mathrm{T},i}$ defines a plane, the intersection point $S_{\mathrm{T},j}$ can occur outside of $\mathcal{T}_{\mathrm{T},i}$ (e.g., $S_{\mathrm{T},i}$) in which case the line $\mathcal{L}_j$ does not intersect $\mathcal{T}_{\mathrm{T},i}$ (note that not all triangles in the surface model are being intersected by a line). It is possible to verify that $S_{\mathrm{T},j}$ is inside $\mathcal{T}_{\mathrm{T},i}$ by summing the angles between the vectors from $S_{\mathrm{T},j}$ to the vertices of triangle $\mathcal{T}_{\mathrm{T},i}$ (the sum of the angles is 2π if $S_{\mathrm{T},j}$ is within the triangle) or in a more computationally efficient way by calculating the area of the triangles transcribed by the vectors (the norm of the cross product of two vectors is equal to twice the area of the triangle transcribed by the vectors). This process is performed for each line in $\mathcal{L}$ for both $\mathcal{M}_{\mathrm{F}}$ and $\mathcal{M}_{\mathrm{T}}$. The results are a set of points, $S_{\mathrm{T},j}$ and $S_{\mathrm{F},j}$, corresponding to the intersection of line $\mathcal{L}_j$ with the tibia and femur surface models, respectively.

(e) Check for minimum distance according to Eq. (3) and set contact points to be $\mathcal{P}_{\mathrm{C.T},k}$, and $\mathcal{P}_{\mathrm{C.F},k}$ $(k = 1,\ldots,w)$.

(f) In case of multiple potential contact points or overlapping surface models due to measurement error (this case is discussed in Sect. 2.2), the contact point is set to be the center of gravity of the contact region.

(g) Transform the tibia surface model $\mathcal{M}_{\mathrm{T}}$ and $\mathcal{L}$ to the next knee configuration such that:

$$ \mathcal{M}_{\mathrm{T},i+1} = {}^{\mathrm{F}}T_{\mathrm{T},i}\mathcal{M}_{\mathrm{T},i} \tag{7} $$

where ${}^{\mathrm{F}}T_{\mathrm{T},i}$ is given in Eq. (4). $\mathcal{L}$ can be transformed as a set of *Plücker* line coordinates [6, 22]:

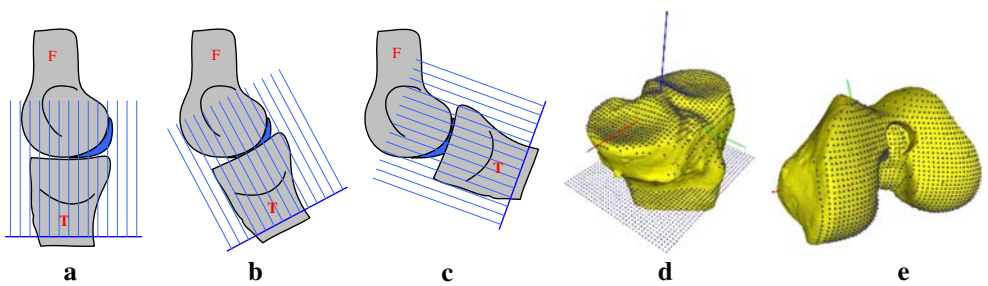

Fig. 1 **a–c** Grid of lines attached to tibia for three different values of flexion, **d**, **e** Sampling grid on the tibia surface model and the points of intersection of the grid lines with tibia surface model, and points of intersection of the grid lines with the femur surface model

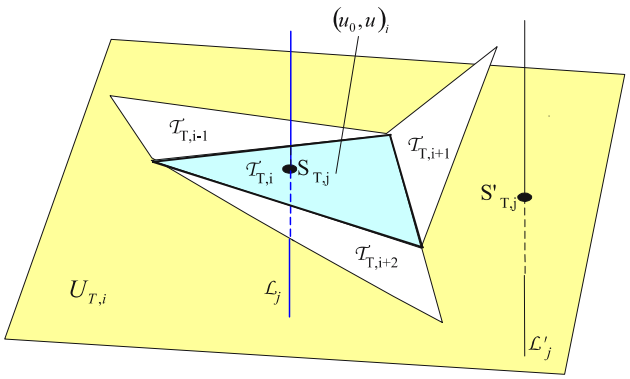

Fig. 2 Example of intersection point $S_{T,j}$ of lines $\mathcal{L}_j$ with triangle '$\mathcal{T}_{T,i}$ in a tibia surface model

$$\mathcal{L}_{i+1} = \begin{bmatrix} R & 0 \\ W \cdot R & R \end{bmatrix} \cdot \mathcal{L}_i^T \tag{8}$$

where W is a skew symmetric matrix given by:

$$W = \begin{bmatrix} 0 & -t_z & t_y \\ t_z & 0 & -t_x \\ -t_y & t_x & 0 \end{bmatrix}, \tag{9}$$

and both R and t are given in Eq. (4). Repeat steps (e)–(g) for each of the w positions.

2.2 Calculating overlap between two surface models

Bone surface model overlap can occur as a result of measurement error or unfeasible solution of joint configuration based on optimization of a kinematic model of the joint (e.g., Fig. 3). In this case, the algorithm is modified as follows:

(a) Follow steps (a)–(d) given in Sect. 2.1.
(b) For each line $\mathcal{L}_j$ calculate:

$$\begin{aligned} d_{T,j} &= \left\| \mathcal{P}_{G,j} - S_{T,j} \right\|_{j=1,\ldots,m} \\ d_{F,j} &= \left\| \mathcal{P}_{G,j} - S_{F,j} \right\|_{j=1,\ldots,m} \end{aligned} \tag{10}$$

(c) For each line, $\mathcal{L}_j$, check whether $d_{T,j} > d_{F,j}$ (e.g., $\mathcal{L}_3 - \mathcal{L}_6$ in Fig. 3). If this is true, then there is penetration of the two surface models. In the case where $d_{T,j} < d_{F,j}$ (e.g., $\mathcal{L}_2$,$\mathcal{L}_{7-8}$ Fig. 3), there is no penetration of the surface models. The lines are modeled as a cuboid with cross-sectional area a. The volume associated with the penetration is given by the sum of the cuboids:

$$V_{\text{total}} = \sum_{j=1}^{m} v_j \tag{11}$$

where

$$v_j = \begin{Bmatrix} a \cdot (d_{T,j} - d_{F,j}) & d_{T,j} > d_{F,j} \\ 0 & d_{T,j} \mathrm{F}, j \end{Bmatrix} \tag{12}$$

2.3 Experimental setting—Sawbones®

For the experiment we used Sawbones® models of the femur and tibia. Prior to the experiment, both bone models were scanned by CT and surface models were generated. The two bone models were then connected by four rubber tubes to simulate the lateral collateral ligament, medial collateral ligament, posterior cruciate ligament, and the anterior cruciate ligament (Fig. 4). Optical trackers were attached to both bones models (Fig. 4), and the surface registration procedure between tracking system and bone models was performed [8]. Both bone models were then tracked throughout the experiment. The femur was rigidly fixed and used as the reference system (Fig. 4), while the tibia was moved from flexion to full extension by quasi-statically pulling it by a wire connected to its center of mass. The tracking system provided the relative positions of the tibia

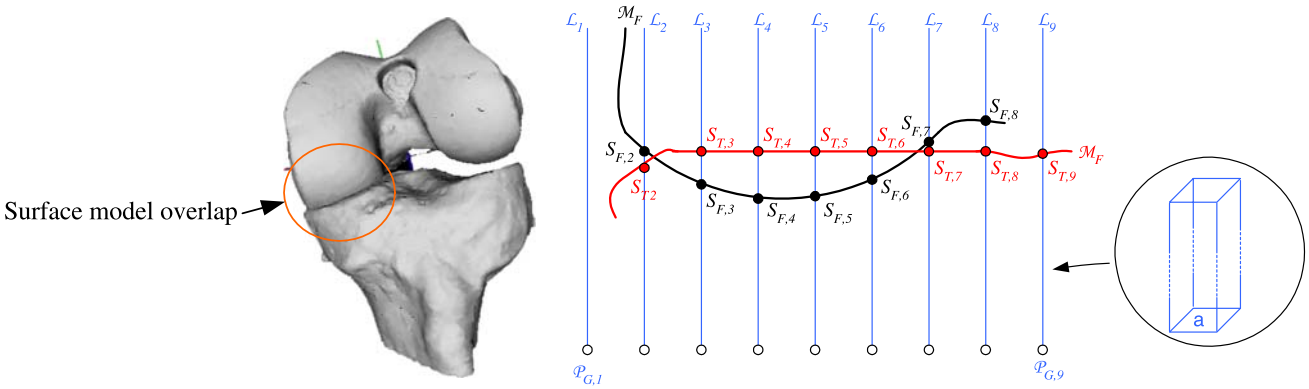

Fig. 3 Example of overlap between two surface models. The *red line* represents the tibia plateau, the *black* line represents the femur

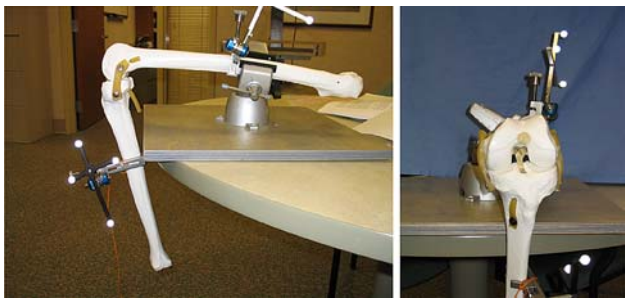

Fig. 4 Observation while flexing the tibia

and femur, i.e., the transformation matrices given in Eq. (4). Next we utilized the algorithm described in Sect. 2.1 to solve for the contact points between the two bones. We also simulated cases where bone overlap occurred and applied the algorithm as described in Sect. 2.2 to resolve the overlap volume between the two surface models.

2.4 Experimental setting—Cadaver

Following the Sawbones® experiment, we ran a set of tests on two cadaver right knees (Fig. 5). Similar to the Sawbones® experiment, both bone models were scanned by CT and surface models were generated. Optical trackers were attached to both bones models (Fig. 5), followed by a surface registration procedure. During experiment the tibia was manipulated while its tracker positions were recorded in the femur tracker reference frame.

3 Results

3.1 Sawbones® model

The contact points were obtained by applying the algorithm described in Sect. 2.1. The results obtained by applying

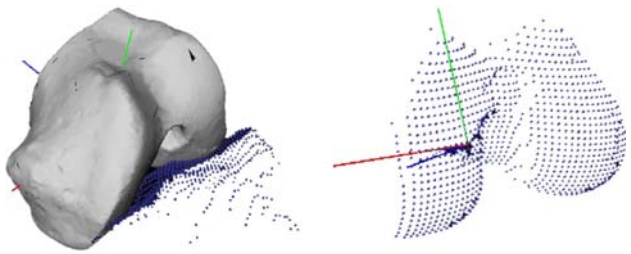

Fig. 6 Intersecting points of $\mathcal{L}$ with $\mathcal{M}_F$

steps (a)–(d) are shown in Fig. 6 and Fig. 1d, e. In Fig. 1d, e one can detect the sampling grid $\mathcal{P}_G$ and the intersection points $S_{T,j}$ and $S_{F,j}$ of the set of lines $\mathcal{L}$ associated with $\mathcal{P}_G$ and the tibia surface model $\mathcal{M}_T$ and femur surface model $\mathcal{M}_F$.

The resulting contact points $\mathcal{P}_{C.T}$ and $\mathcal{P}_{C.F}$ are calculated in step (e). The resulting contact points for the entire flexion motion are given in Fig. 7. This set of points is also characterized as the contact path [5].

Next, we applied the algorithm given in Sect. 2.2 to evaluate the surface model overlap. We used the bone configuration given in Fig. 4 as an input to the algorithm. Rather than obtaining a contact path, the algorithm, as expected, identified a contact region on the medial condyle (Fig. 8). When applying step (c) and Eq. (11), a 15.1 mm^3 volumetric intersection between the two surface models is obtained. For this simulation we used a grid where $d_x = d_y = 1.5\,mm$ (average area of triangles in the surface models was 1 mm).

3.2 Cadavers

Contact points for the cadaver experiment for different flexion angles are given in Fig. 9. These results depend on the cartilage; however, the proposed method can provide initial solutions for calculating accurate contact path taking also into account the cartilage deflection.

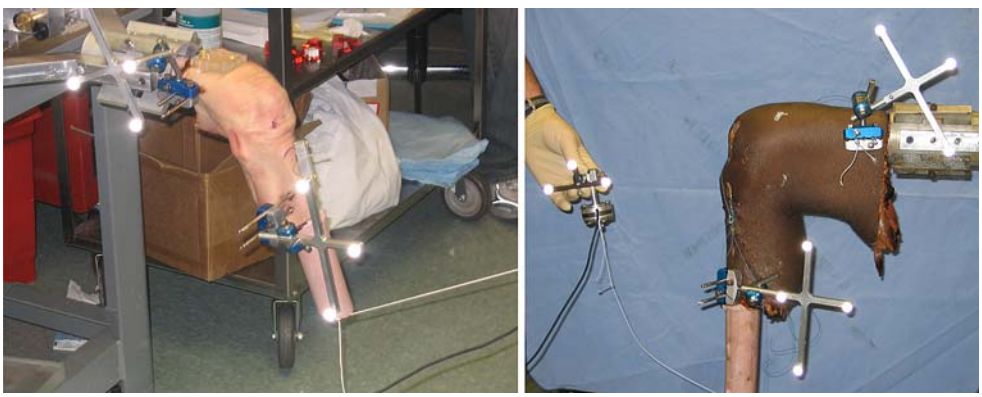

Fig. 5 Experimental setting; Male, 81 (*left*), Male, 68 (*right*)

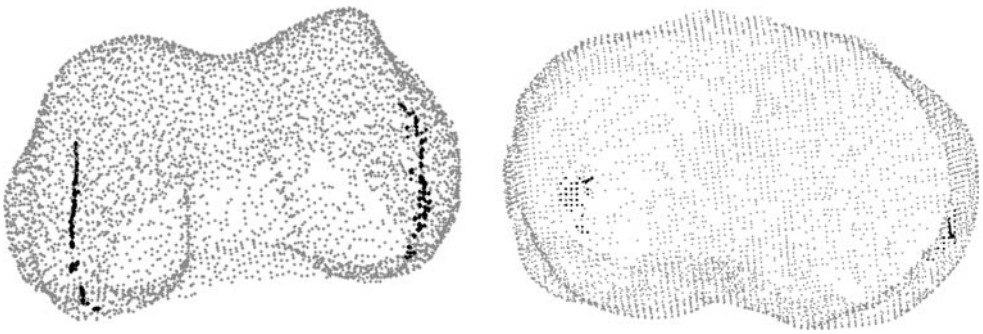

Fig. 7 Articular contact path from Sawbones® experiment on femur and tibia

4 Discussion

This study describes a fully automated computer algorithm for detecting contact points between surface models of the tibia and femur while subjected to flexion/extension motion. The general idea behind the algorithm is to attach a predetermined grid of lines to the moving bone (tibia) and use basic tools from computational line geometry to represent the grid lines, and calculate the line-surface intersections.

We also described an extension to the algorithm that results in a volumetric estimation of bone overlap in the case of two surface models that overlap each other. This could be a result of measurement errors or a result from an optimization procedure that calculates relative bone positions based on biomechanical models of the knee. Overlap may also occur when trying to predict joint motion based on a computer model of the geometry, and hard tissue and soft tissue mechanical properties. These models usually solve the joint kinematics based on optimization of an objective function. In the case where bone overlap is not compensated for in the objective function, e.g., as a penalty, the optimization algorithm can result in unfeasible configurations where bones overlap.

The suggested algorithm is general and can be applied, with minor adjustments, to any joint or two surface models that move with respect to each other providing that the contact surfaces are sufficiently rigid. The planar grid concept can be extended to work with a non-planar geometry, such as a grid on spherical surface where the line direction is defined normal to the spherical surface. The user would just have to adjust the default grid location and the logic of what defines a valid intersection (how and where to look for the intersection). Finally, one needs to determine the grid spacing. Grid spacing depends upon the required output resolution, input surface model resolution, and computation time. Once these parameters are determined the algorithm is fully automated and does not require an interface or input from the user during the process.

In the case of deformable contact, this approach can be used as a starting point. Previous studies have used different techniques to identify contact mechanics of joints, such as using sensitive pressure films [13, 14], electronic pressure transducers [10, 24], MRI scans [7, 11, 21, 23], CT scans [1, 18] and biomechanical simulations [5]. The main advantage of the proposed method is that data can be obtained using simple optical tracking hardware and surface models of the object. Moreover, once observational data are obtained from the tracking system and surface models are available, the algorithm generates the results without any further interaction or input from the user. This makes the proposed algorithms ideal for use in

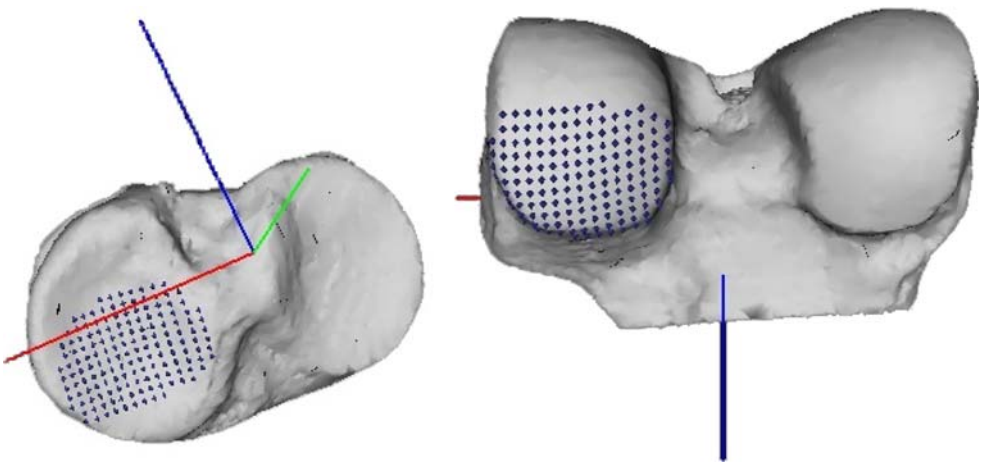

Fig. 8 Contact region in case of surface models overlap

Fig. 9 Contact points (path) as calculate for different flexion angles of the tibia

biomechanical studies, simulations and optimizations of joint kinematics.

Acknowledgments This work was supported by the National Science Foundation of the United States under NSF ITR Grant No. 0325920.

References

1. Asano T, Akagi M, Tanaka K, Tamura J, Nakamura T (2001) In vivo three dimensional knee kinematics using a biplanar image-matching techniques. Clin Orthop 388:157–166
2. Bansk S, Hodge WA (1996) Accurate measurement of three-dimensional knee replacement kinematics using single plane fluoroscopy. IEEE Trans Biomed Eng 43:638–649
3. Banks S, Markovich GD, Hodge WA (1997) In vivo kinematics of cruciate-retaining and substituting knee arthroplasties. J Arthroplasty 12:297–304
4. Blankevoort L, Kuiper JH, Huiskes R, Grootenboer HJ (1991) Articular contact in a three-dimensional model of the knee. J Biomech 24:1019–1031
5. Chen E, Ellis RE, Bryant JT, Rudan JF (2001) A computational model of postoperative knee kinematics. Med Image Anal 5:317–330
6. Davidson JK, Hunt KH (2004) Robots and screw theory, application of kinematics and statics to robotics. Oxford University Press, New York,
7. DeFrate LE, Sun H, Gill TJ, Rubash HE, Li G (2004) In vivo tibiofemoral contact analysis using 3D MRI-based knee models. J Biomech 37:1499–1504
8. DiGioia AM, Jaramaz B, Blackwell M, Simon DA, Fritz M, Moody JE, Nikou C, Colgan BD, Aston MA, Labaraca RS, Kischell E, Kanade T (1998) The Otto Aufrance award: image guided navigation system to measure intraoperatively acetabular implant alignment. Clin Orthop 355:8–22
9. Essinger JR, Leyvaraz PF, Heegard HJ, Robertson DD (1989) A mathematical model for the evaluation of the behaviour during flexion of condylar-type knee prostheses. J Biomech 22:1229–1241
10. Greis PE, Scuderi MG, Mohr A, Bachus KN, Burks RT (2002) Glenohumeral articular contact areas and pressures following labral and osseous injury to the anteroinferior quadrant of the glenoid. J Shoulder Elbow Surg 11:442–451
11. Heino BJ, Powers CM, Terk MR, Ward SR, Lee TQ (2003) Quantification of the patellofemoral joint contact area using magnetic resonance imaging. Magn Reson Imaging 21:955–959
12. Hoff WA, Komistek RD, Dennis DA, Gabriel SM, Walker SA (1996) Three-dimensional determination of femoral–tibial contact positions under "in vivo" conditions using fluoroscopy. In: Proceedings of the European society of biomechanics, Leuven, pp 28–31
13. Hsieh YF, Draganich LF, Ho SH, Reider B (2002) The effect of removal and reconstruction of the anterior cruciate ligament on the contact characteristics of the patellofemoral joint. Am J Sports Med 30:121–127
14. Huberti HH, Hayes WC (1984) Patellofemoral contact pressures. The influence of q-angle and tendofemoral contact. J Joint Bone Surg A 66:715–724
15. Invaco SJ, Mullins E, Coughlin KM, Banks S, Banks A, Beynnon BD (2004) Tibiofemoral kinematic analysis of kneeling after total knee arthroplasty. J Arthroplasty 19:906–910
16. Klein F (1871) Ueber Liniengeometrie und metrische Geometrie. Mathematische Annalen v, pp 257–303
17. Komistek RD, Scott RD, Dennis DA, Yasgur D, Anderson DT, Hajner ME (2002) In vivo comparison of femorotibial contact positions for press fit posterior stabilized and posterior cruciate-retaining total knee arthroplasties. J Arthroplasty 17:209–216

18. Komistek RD, Dennis DA, Mahfouz M (2003) In vivo fluoroscopic analysis of the normal human knee. Clin Orthop 410:69–81
19. Pottmann H, Wallner J (2001) Computational line geometry. Springer, Berlin
20. Pottmann H, Peternell M, Ravani B (1999) An introduction to line geometry with applications. Comput Aided Des 31:3–16
21. Scarvell JM, Smith PN, Refshauge KM, Galloway HR, Woods KR (2004) Evaluation of a method to map tibiofemoral contact points in the normal knee using MRI. J Orthop Res 22:788–793
22. Tsai LW (1999) Robot analysis: the mechanics of serial and parallel manipulators. Wiley, New York
23. Von Eisenhart-Rothe R, Siebert M, Bringmann C, Vogl T, Englmeier KH, Graichen H (2004) A new in vivo technique for determination of 3D kinematics and contact areas of the patellofemoral and tibio-femoral joint. J Biomech 37:927–934ssss
24. Wilson DR, Apreleva MV, Eichler MJ, Harrold FR (2003) Accuracy and repeatability of the pressure measurement system in the patellofemoral joint. J Biomech 36:1909–1915
25. Wismans J, Veldpaus F, Janssen J (1980) A three-dimensional mathematical model of the knee-joint. J Biomech 13:677–685